

Correlation between Crystal Structure and Mobility in Organic Field-Effect Transistors Based on Single Crystals of Tetrathiafulvalene Derivatives

Marta Mas-Torrent,^{*,†} Peter Hadley,[†] Stefan T. Bromley,[‡] Xavi Ribas,[§] Judit Tarrés,[§] Montserrat Mas,[§] Elies Molins,[§] Jaume Veciana,[§] and Concepció Rovira^{*,§}

Contribution from the Kavli Institute of NanoScience, Delft University of Technology, Lorentzweg 1, 2628 CJ Delft, The Netherlands, Ceramic Membrane Centre "The Pore", Delft University of Technology, Julianalaan 136, 2628 BL Delft, The Netherlands, and Institut de Ciència de Materials de Barcelona, Campus de la Universitat Autònoma de Barcelona, 08193 Bellaterra, Spain

Received March 23, 2004; E-mail: marta@qt.tn.tudelft.nl; cun@icmab.es

Abstract: Recently, it was reported that crystals of the organic material dithiophene-tetrathiafulvalene (DT-TTF) have a high field-effect charge carrier mobility of $1.4 \text{ cm}^2/(\text{V}\cdot\text{s})$. These crystals were formed by a simple drop-casting method, making this material interesting to investigate for possible applications in low-cost electronics. Here, organic single-crystal field-effect transistors based on materials related to DT-TTF are presented and a clear correlation between the crystal structure and the electrical characteristics is observed. The observed relationship between the mobilities in the different crystal structures is strongly corroborated by calculations of both the molecular reorganization energies and the maximum intermolecular transfer integrals. The most suitable materials described here exhibit mobilities that are among the highest reported for organic field-effect transistors and that are the highest reported for solution-processed materials.

Introduction

Organic field-effect transistors (OFETs) have attracted a great deal of interest over the past few years due to their unique processing characteristics and improved electronic mobility.¹ Thus far, most of the OFETs investigated have been prepared from spin-coated polymers and vapor-deposited films of low-molecular-weight species. The intermolecular disorder present in these films limits the charge carrier mobility of the resulting devices,² and thus, much effort has been devoted to improving the organic thin-film quality.^{3,4} The fundamental material characteristics of organic semiconductors are most clearly measured in single crystals,^{5–8} where the highest mobilities are observed. Mobilities of 1.5 and $15 \text{ cm}^2/(\text{V}\cdot\text{s})$ have been reported for pentacene⁹ and rubrene,⁶ respectively. Several approaches

have been tried to improve the quality of the materials further as purifying the materials is important to achieve high mobilities. Some attempts have focused on directly functionalizing pentacene, the benchmark in organic semiconductors, in order to tune its electronic properties¹⁰ or to impart solubility and/or enhance the intermolecular overlap.^{11,12} Also, various oligothiophene derivatives have been studied in order to relate their molecular structure with their electronic properties.^{4,13–14} However, despite the high number of organic semiconductors that have been evaluated so far and the recent studies on the effect of molecular orientation on electrical characteristics,^{3,15–17} there remains a

[†] Kavli Institute of NanoScience, Delft University of Technology.

[‡] Ceramic Membrane Centre "The Pore", Delft University of Technology.

[§] Institut de Ciència de Materials de Barcelona.

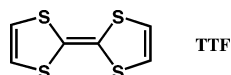
- (1) Dimitrakopoulos, C. D.; Malenfant, P. R. L. *Adv. Mater.* **2002**, *14*, 99–117.
- (2) Campbell, I. H.; Smith, D. L. *Solid State Phys.* **2001**, *55*, 1.
- (3) Noh, Y.-Y.; Kim, J.-J.; Yoshida, Y.; Yase, K. *Adv. Mater.* **2003**, *15*, 699–702.
- (4) Yanagi, H.; Araki, Y.; Ohara, T.; Hotta, S.; Ichikawa, M.; Taniguchi, Y. *Adv. Funct. Mater.* **2003**, *13*, 767–773.
- (5) (a) Podzorov, V.; Sysoev, S. E.; Loginova, E.; Pudalov, V. M.; Gershenson, M. E. *Appl. Phys. Lett.* **2003**, *83*, 3504–3506. (b) Sundar, V. C.; Zaumseil, J.; Podzorov, V.; Menard, E.; Willett, R. L.; Someya, T.; Gershenson, M. E.; Rogers, J. A. *Science* **2004**, *303*, 1644–1646.
- (6) De Boer, R. W. I.; Klapwijk, T. M.; Morpurgo, A. F. *Appl. Phys. Lett.* **2003**, *83*, 4345–4347.
- (7) Ichikawa, M.; Yanagi, H.; Shimizu, Y.; Hotta, S.; Sugauma, N.; Koyama, T.; Taniguchi, Y. *Adv. Mater.* **2002**, *14*, 1272–1275.
- (8) Butko, V. Y.; Chi, X.; Lang, D. V.; Ramirez, A. P. *Appl. Phys. Lett.* **2003**, *83*, 4773–4775.

- (9) Nelson, S. F.; Lin, Y.-Y.; Gundlach, D. J.; Jackson, T. N. *Appl. Phys. Lett.* **1998**, *72*, 1854–1856.
- (10) Meng, H. M.; Bendikov, M.; Mitchell, G.; Helgeson, R.; Wudl, F.; Bao, Z.; Siegrist, T.; Kloc, C.; Chen, C.-H. *Adv. Mater.* **2003**, *15*, 1090–1093.
- (11) (a) Anthony, J. E.; Brooks, J. S.; Eaton, D. L.; Parkin, S. R. *J. Am. Chem. Soc.* **2001**, *123*, 9482–9483. (b) Anthony, J. E.; Eaton, D. L.; Parkin, S. R. *Org. Lett.* **2002**, *4*, 15–18.
- (12) (a) Herwig, P. T.; Müllen, K. *Adv. Mater.* **1999**, *11*, 480–483. (b) Gelink, G. H.; Huitema, H. E. A.; van Veenendaal, E.; Cantatore, E.; Schrijnemakers, L.; van der Putten, J. B. P. H.; Geuns, T. C. T.; Beenhakkers, M.; Giesbers, J. B.; Huisman, B.-H.; Meijer, E. J.; Mena Benito, E.; Touwslager, F. J.; Marsman, A. W.; van Rens, B. J. E.; de Leeuw, D. M. *Nat. Mater.* **2004**, *3*, 106–110. (c) Afzali, A.; Dimitrakopoulos, C. D.; Breen, T. L. *J. Am. Chem. Soc.* **2002**, *124*, 8812–8813.
- (13) Halik, M.; Klauk, H.; Zschieschang, U.; Schmid, G.; Ponomarenko, S.; Kirchmeyer, S.; Weber, W. *Adv. Mater.* **2003**, *15*, 917–922.
- (14) Vidlot, C.; Ackermann, J.; Blanchard, P.; Raimundo, J.-M.; Frère, P.; Allain, M.; de Bettignies, R.; Levillain, E.; Roncali, J. *Adv. Mater.* **2003**, *15*, 306–310.
- (15) Sirringhaus H.; Brown P. J.; Friend R. H.; Nielsen M. M.; Bechgaard K.; Langeveld-Voss B. M. W.; Spiering A. J. H.; Janssen R. A. J.; Meijer E. W.; Herwig P. *Nature* **1999**, *401*, 685–688.
- (16) Ponomarenko, S. A.; Kirchmeyer, S.; Elschner, A.; Huisman, B.-H.; Karbach, A.; Drechsler, D. *Adv. Funct. Mater.* **2003**, *13*, 591–596.
- (17) Nagamatsu, S.; Tanigaki, N.; Yoshida, Y.; Takashima, W.; Yase, K.; Kaneto, K. *Synth. Met.* **2003**, *137*, 923–924.

lack of understanding of the relationship between crystal structure and field-effect mobility, which is crucial for the future design of new materials.¹⁸

Recently, we reported a very high mobility of 1.4 cm²/(V·s) for a dithiophene-tetrathiafulvalene (DT-TTF) single-crystal transistor.¹⁹ This device, in contrast to previously reported single-crystal devices, in which the crystals are grown from the vapor phase in long experiments, was prepared using a simple room-temperature drop-casting technique, which makes it interesting for applications in low-cost electronics. The outstanding device performance and the fact that TTF derivatives can be easily processed open new perspectives in the field of OFETs.

In this paper we report on a systematic study of the dependency of the charge carrier mobility of single-crystal OFETs based on tetrathiafulvalene (TTF) derivatives on the crystal structure. The comparison of the devices' performances using crystals of very similar molecules but with different crystal packing allows for the focused investigation of the influence of the intermolecular interactions on the electronic transport properties.



Results and Discussion

We studied seven different TTF derivatives, which are shown in Figure 1, namely bis(ethylenedithio)-tetrathiafulvalene (BEDT-TTF), (ethylenethio)(ethylenedithio)-tetrathiafulvalene (ETEDT-TTF), bis(ethylenethio)-tetrathiafulvalene (BET-TTF), (ethylenethio)(thiodimethylene)-tetrathiafulvalene (ETTDM-TTF), dithiophene-tetrathiafulvalene (DT-TTF), (thiophene)(thiodimethylene)-tetrathiafulvalene (TTDM-TTF), and (ethylenethio)(thiophene)-tetrathiafulvalene (ETT-TTF). The symmetric TTF derivatives BEDT-TTF, BET-TTF, and DT-TTF were chosen to compare different types of crystal structures. The related derivatives ETEDT-TTF, ETTDM-TTF, TTDM-TTF, and ETT-TTF were chosen due to their lower symmetry in order to compare not only the effect of structural variability but also the effect of disorder on the observed charge carrier mobilities. The π -electron donors ETTDM-TTF and TTDM-TTF and their crystal structures are described herein for the first time (see Experimental Section). Taking into account the crystal packing in which these molecules are arranged, this family of compounds can be classified into three different groups, each group containing symmetric and related disymmetric TTF derivatives.

The first group (**G1**) consists of the symmetric molecule BEDT-TTF²⁰ and the disymmetric derivative ETEDT-TTF.²¹ Both molecules deviate significantly from planarity, as a folding of the dithiolenes along the S···S hinge and a boat conformation of the six-membered rings are observed. Similar to BEDT-TTF, the supramolecular organization of ETEDT-TTF consists

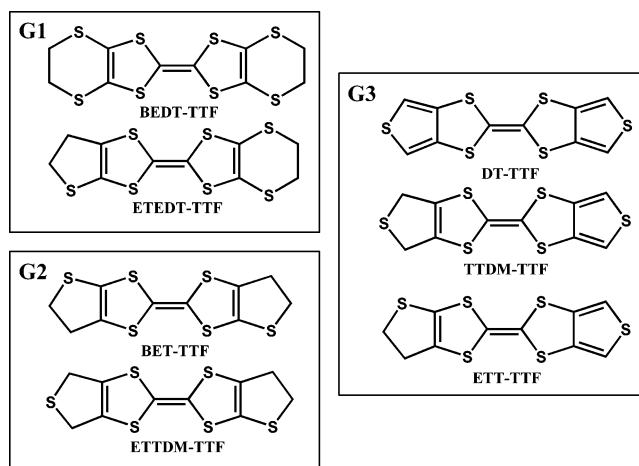


Figure 1. Molecular structures of the studied TTF derivatives.

of head-to-tail dimers sustained by C—H···S and C—H···C hydrogen bonds, forming chains along the *a* direction due to multiple lateral S···S contacts ($3.56 \text{ \AA} < d(\text{S}\cdots\text{S}) < 3.82 \text{ \AA}$; see Figure 2). These chains are arranged perpendicularly to each other, avoiding the overlap of the dimers to form stacks (Figure 2a). Although the formation of dimers in the crystals of both BEDT-TTF and ETEDT-TTF interrupts the HOMO–HOMO interactions between them, there are numerous lateral S···S short intermolecular interactions along the *a* axis.^{20b} The main difference between the BEDT-TTF and ETEDT-TTF crystal structures is the disorder of the ethylenethio groups (59–41%) in ETEDT-TTF.²¹

BET-TTF^{22,20b} and ETTDM-TTF²³ belong to the second crystal structure group (**G2**). The crystal packing of these compounds can be described as being built up from series of chains of quasi planar molecules along the *a* axis interacting side-by-side. These chains stack into layers in such a way that the molecules in one chain are shifted along the direction of the long molecular axis with respect to those in adjacent chains. The molecules of every layer are also displaced with respect to those of adjacent layers. BET-TTF and ETTDM-TTF structures differ in that molecules of BET-TTF in one chain are shifted along the direction of the short molecular axis with respect to those in adjacent chains, whereas in ETTDM-TTF this displacement is insignificant and shows a better interplanar overlap. Besides, in ETTDM-TTF the stacked chains allow for the formation of dimers along the *b* axis, which is not observed in BET-TTF. The interplanar distance between molecules in the same layer is 3.618 Å in BET-TTF and 3.568 and 3.663 Å in ETTDM-TTF, for the intradimer and interdimer distances, respectively (Figure 3a). Very short intermolecular S···S contacts ($3.46 \text{ \AA} < d(\text{S}\cdots\text{S}) < 3.56 \text{ \AA}$ for BET-TTF; $3.60 \text{ \AA} < d(\text{S}\cdots\text{S}) < 3.61 \text{ \AA}$ for ETTDM-TTF) between molecules belonging to parallel stacks are found in the *ab* plane for BET-TTF and in the *ac* plane for ETTDM-TTF (Figure 3b). Previous calculations of the intermolecular interaction energies in BET-TTF crystals reveal that there are important electronic interactions in almost all the directions of the crystal, which leads to a dispersive HOMO band.²⁴ Although the crystal structure of

(18) (a) Curtis, M. D.; Cao, J.; Kampf, J. W. *J. Am. Chem. Soc.* **2004**, *126*, 4318–4328. (b) Koren, A. B.; Curtis, M. D.; Francis, A. H.; Kampf, J. W. *J. Am. Chem. Soc.* **2003**, *125*, 5040–5050.

(19) Mas-Torrent, M.; Durkut, M.; Hadley, P.; Ribas, X.; Rovira, C. *J. Am. Chem. Soc.* **2004**, *126*, 984–985.

(20) (a) Kobayashi, H.; Kobayashi, A.; Sasaki, Y.; Saito, G.; Inokuchi, H. *Bull. Chem. Soc. Jpn.* **1986**, *59*, 301. (b) Novoa, J. J.; Rovira, M. C.; Rovira, C.; Veciana, J.; Tarrés, J. *Adv. Mater.* **1995**, *7*, 233–237.

(21) Ribera, E.; Veciana, J.; Molins, E.; Mata, I.; Wurst, K.; Rovira, C. *Eur. J. Org. Chem.* **2000**, 2867–2875.

(22) Rovira, C.; Veciana, J.; Santaló, N.; Tarrés, J.; Cirujeda, J.; Molins, E.; Llorca, J.; Espinosa, E. *J. Org. Chem.* **1994**, *59*, 3307–3313.

(23) Synthesis and X-ray crystallographic data of ETTDM-TTF are described in the Experimental Section.

(24) Rovira, M. C.; Novoa, J. J.; Tarrés, J.; Rovira, C.; Veciana, J.; Yang, S.; Cowan, D. O.; Canadell, E. *Adv. Mater.* **1995**, *7*, 1023–1027.

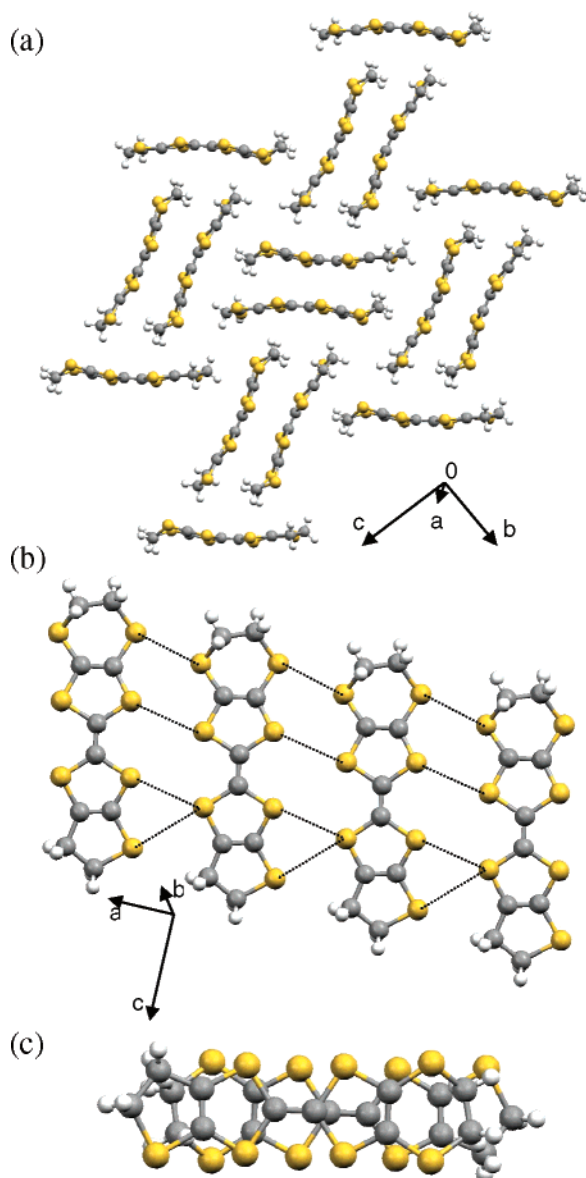


Figure 2. Crystal structure of the disymmetric ETEDT-TTF, representative of group 1: (a) view perpendicular to the TTF core plane, (b) chains along the *a* axis through S...S contacts (dotted lines), and (c) overlap within the dimerized molecules.

BET-TTF shows that there is disorder of the ethylenethio groups (15%) due to positional disorder or cis/trans isomerism, calculations indicate that such disorder does not decrease the strength of the interaction energies.²⁴ Similar disorder of the ethylenethio groups (20%) is found in the crystal structure of ETTDM-TTF, for which the interaction energies strength is also assumed to be unaffected.

Finally, the third group (**G3**) consists of DT-TTF,²² TTDM-TTF,²⁵ and ETT-TTF.²⁶ These molecules crystallize forming uniform stacks of almost planar molecules along the *b* axis in a herringbone pattern (Figure 4). The interplanar distance between the molecules along one stack is very short in these crystals (3.56 Å for DT-TTF, 3.59 Å for TTDM-TTF, 3.66 Å

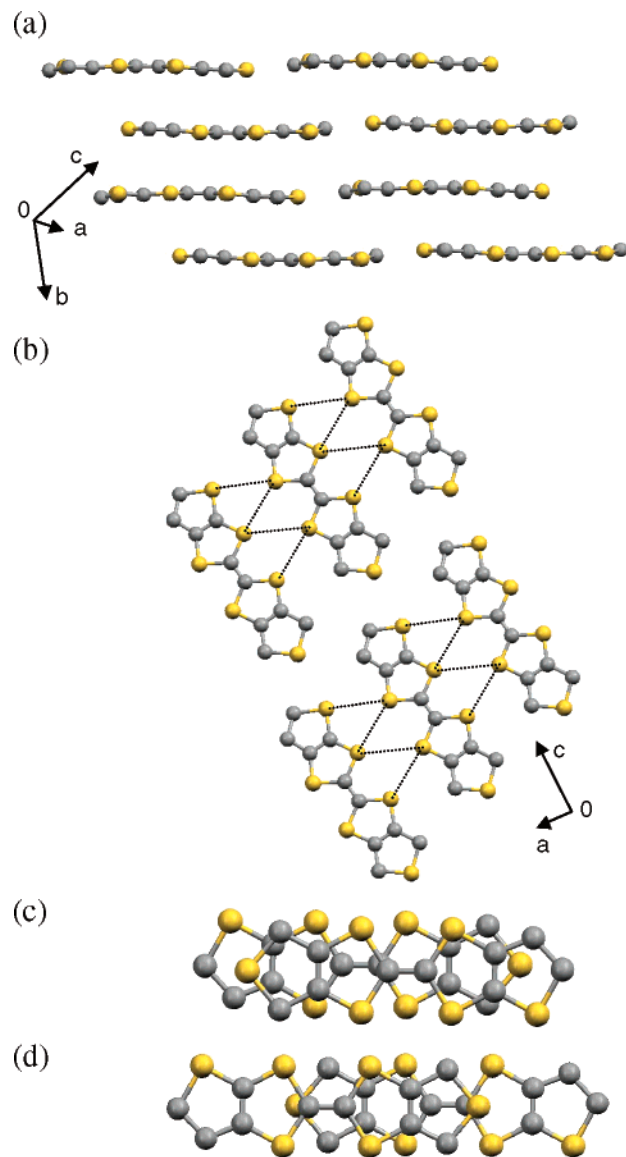


Figure 3. Crystal structure of the disymmetric ETTDM-TTF, representative of group 2: (a) view perpendicular to the stacking axis *b*, (b) view along the stacking axis *b* (S...S contacts in the *ac* plane as dotted lines), (c) intradimer overlap, and (d) interdimer overlap. (Hydrogen atoms have been omitted for clarity.)

for ETT-TTF), exhibiting an effective intrastack molecular overlap. Short intermolecular S...S contacts (3.55 and 3.61 Å for DT-TTF; 3.61 and 3.71 Å for TTDM-TTF; 3.63 and 3.72 Å for ETT-TTF) are found between molecules of different stacks along the *c* axis. The disymmetric molecules TTDM-TTF and ETT-TTF incorporate inherent disorder in the crystal structure. In TTDM-TTF, a 50% disorder is found in the aromaticity of the exocyclic five-membered ring. The crystal packing of ETT-TTF also presents the same disorder, but with the addition of a 25% disorder of the ethylenethio groups, which leads to a significantly disordered structure.

Figure 5a shows the device configuration used for measuring the charge carrier field-effect mobility of the semiconducting TTF derivatives. The organic semiconductor was deposited onto the gate insulator and the prefabricated source and drain electrodes. The electrodes were fabricated by electron-beam lithography on a 200 nm thick oxidized silicon wafer. The electrodes consist of 4 nm of titanium, acting as a sticking layer,

(25) Synthesis and X-ray crystallographic data of TTDM-TTF are described in the Experimental Section. For its use as a π -electron donor, see: Lopes, E. B.; Alves, H.; Ribera, E.; Mas-Torrent, M.; Auban-Senzier, P.; Canadell, E.; Henriques, R. T.; Almeida, M.; Molins, E.; Veciana, J.; Rovira, C.; Jérôme, D. *Eur. Phys. J. B* **2002**, *29*, 27–33.

(26) Tarrés, J. Ph.D. Thesis, University of Barcelona, Barcelona, Spain, 1997.

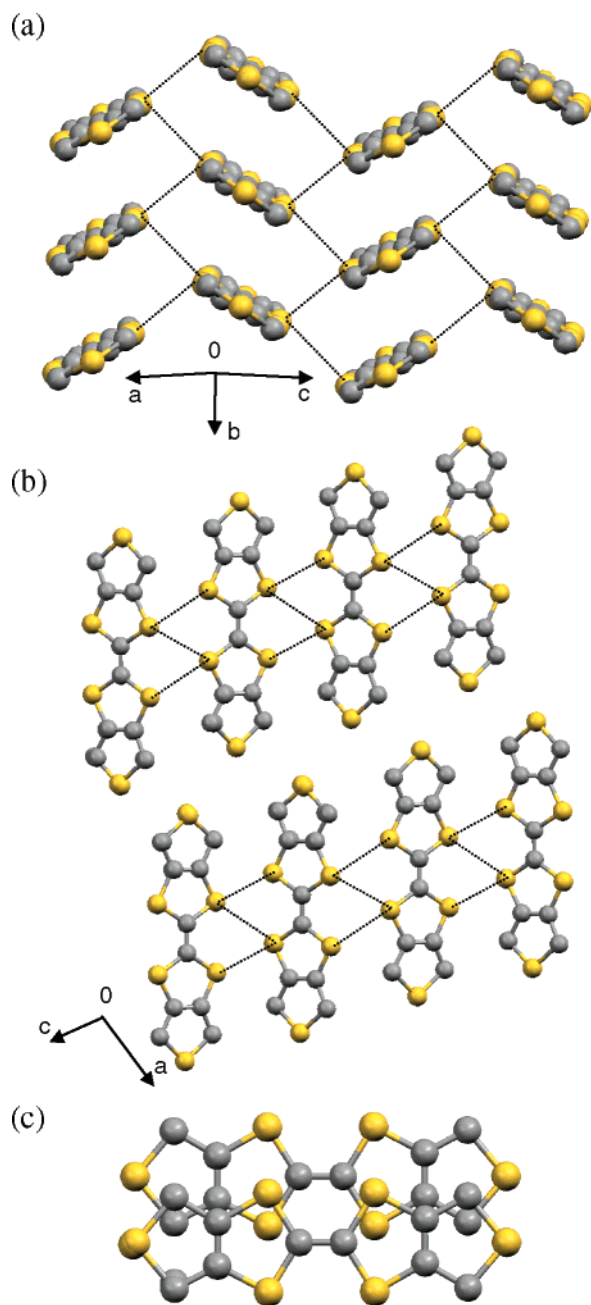


Figure 4. Crystal structure of TTDm-TTF, one of the members of group 3: (a) herringbone stacking pattern, (b) view along the stacking axis *b* (*S*...*S* contacts as dotted lines), and (c) molecular overlap. (Hydrogen atoms have been omitted for clarity.)

covered by 20 nm of gold, and they are spaced 50–300 μm apart. The organic crystals were obtained by drop-casting following the same procedure used for the preparation of DT-TTF single-crystal FETs:¹⁹ a warm saturated solution of the TTF derivative in chlorobenzene was poured over the electrodes and the solvent evaporated at room temperature. This process resulted in the formation of long, thin crystals, some of which connected two of the microfabricated gold electrodes. Figure 5b,c shows two photographs of some of the measured crystals lying across two gold electrodes. Molecules from groups 1 and 3 tend to form long, thin crystals with smooth surfaces. However, we found that the molecules in group 2 have more difficulty in crystallizing; in particular, ETTDM-TTF crystallizes forming dendritic crystals.

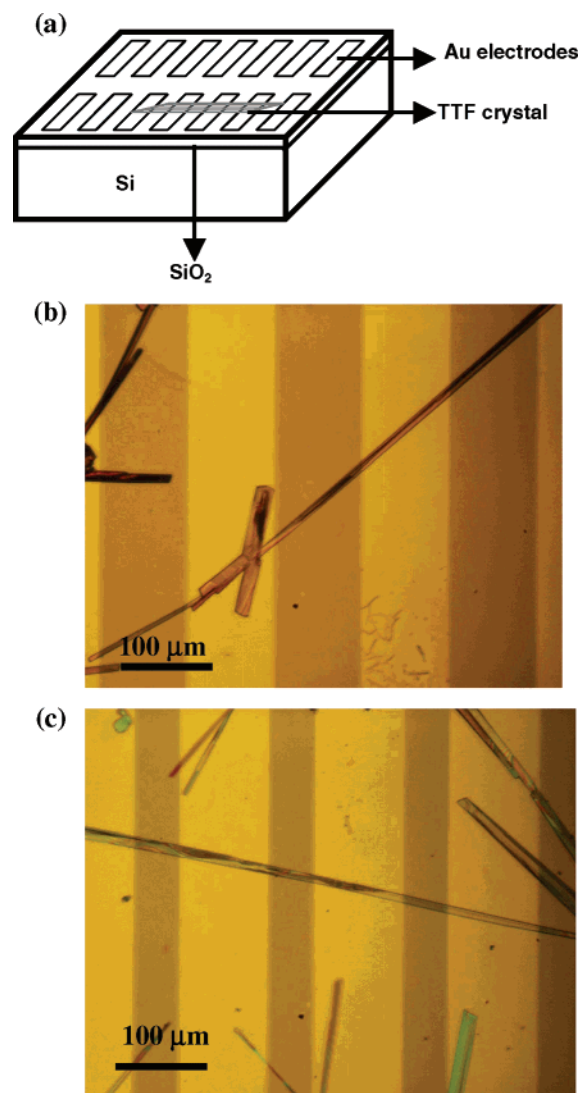


Figure 5. (a) Schematic view of the device configuration used. (b,c) Optical microscopy images of single crystals of (b) ETEDT-TTF and (c) ETT-TTF formed on the microfabricated electrodes.

The electrical characterization of the devices was performed by measuring the source–drain current, I_{SD} , while sweeping the applied source–drain voltage, V_{SD} , across the two electrodes for different gate voltages, V_{G} , applied to the silicon substrate. Figure 6 shows the outcome of the measurements performed on two different devices based on BEDT-TTF and DT-TTF. The resulting graphs obtained for all the devices are typical of a p-type semiconductor. As a more negative V_{G} is applied, more holes are induced in the semiconductor, and the current increases. The field-effect mobility is evaluated in the linear regime of operation by first calculating the conductance ($dI_{\text{SD}}/dV_{\text{SD}}$) of the curves for each V_{G} and then using the formula

$$\mu = \frac{\partial^2 I_{\text{SD}}}{\partial V_{\text{SD}} \partial V_{\text{G}}} \frac{L}{CW}$$

where μ is the mobility, C the capacitance per unit area of the gate, and W and L the width and length of the crystal between the source and drain electrodes, respectively. This formula neglects the influence of contact resistances and charge traps in the gate oxide. In a few cases, four-contact measurements

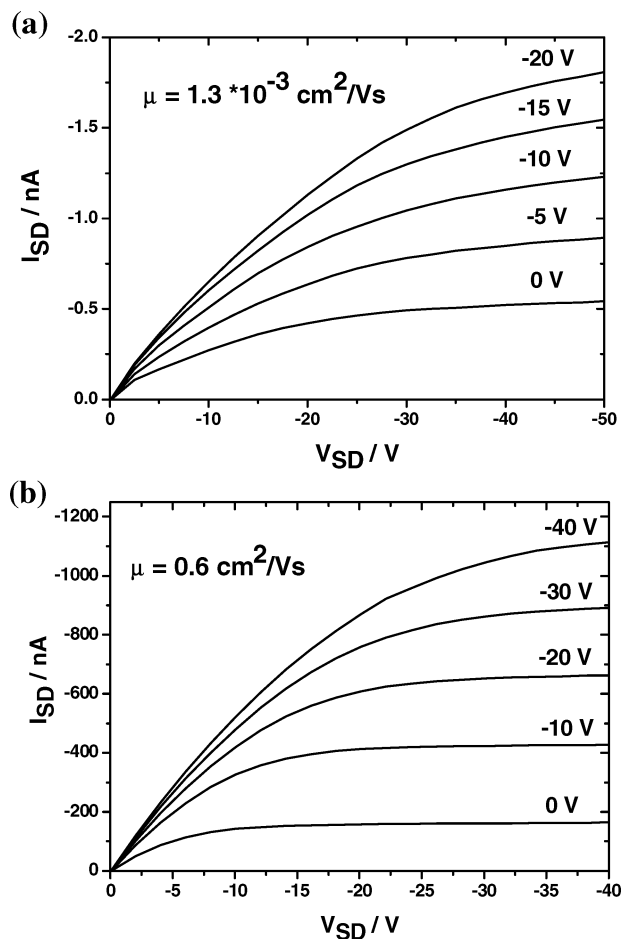


Figure 6. I_{SD} versus V_{SD} at constant V_G for a single-crystal OFET based on (a) BEDT-TTF (this device has a channel length (L) and width (W) of 100 and 7 μm , respectively) and (b) DT-TTF (with $L = 300 \mu\text{m}$ and $W = 60 \mu\text{m}$).

were performed to check the contact resistance. Contact resistances between 3 and 5 $M\Omega$ were registered, which implies that the intrinsic mobility can be up to double the values previously calculated. Consequently, the mobilities reported here, calculated using the above formula, merely provide a lower limit on the device mobility.²⁷

Most of these devices were stable in air for several weeks. Only for a few very thin crystals was there a change in mobility after exposure to air. This indicates that there was some oxidation of the TTF derivative. However, by applying a negative gate voltage, the molecules could be reduced again.²⁸

We measured 67 different single-crystal OFETs using the TTF derivatives mentioned above. The graph in Figure 7 summarizes the mobilities found for all these devices, and the mean values are given in Table 1. The dashed lines in the plot separate the three different groups determined according to their crystal structure (G1–3). Taking into account the distribution in the mobilities for each TTF derivative due to differences in the crystal quality or in the device, it is evident that there is, for all studied crystal groups, a clear correlation between the crystal structure and the device mobilities achieved. Although we should also note that there might be some uncertainty due to the

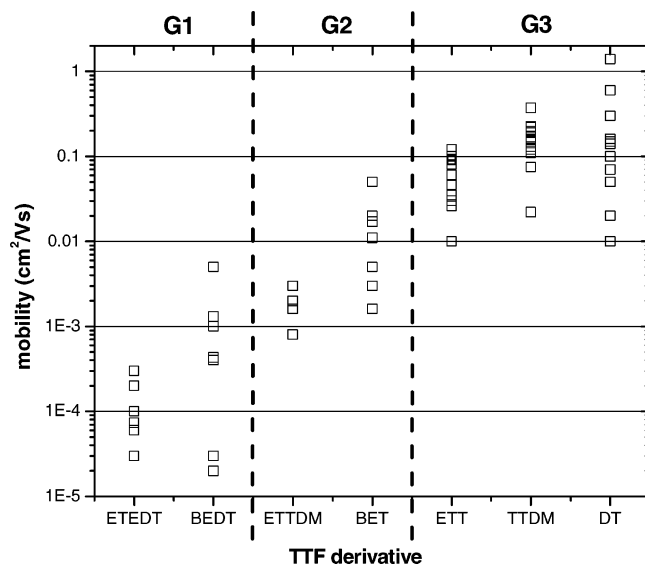


Figure 7. Summary table of the mobilities obtained for the studied TTF derivatives. The dashed lines separate the three groups of molecules considering their crystal structure (G1, G2, and G3).

Table 1. Mean Values of Charge Carrier Mobilities (μ_m) and Their Standard Deviations (in Parentheses), Maximum Transfer Integrals of the Symmetric Derivatives (t_{max}), and Isolated Molecular Reorganization Energies of the TTF Derivatives Using the Minimum Energy Neutral and 1+ Conformations (λ_{reorg}) and Using the Neutral Local Minimum Energy Conformation Best Approximating the Crystal Structure Conformation ($\lambda_{reorg}(c)$)

TTF derivative	μ_m , $\text{cm}^2/(\text{V}\cdot\text{s})$	λ_{reorg} , eV	$\lambda_{reorg}(c)$, eV	t_{max} , eV	
G1	ETEDT-TTF	1.4×10^{-4} (9.8×10^{-5})	0.506	0.488	
	BEDT-TTF	1.2×10^{-3} (1.7×10^{-3})	0.550	0.550	0.019
G2	ETDDM-TTF	1.8×10^{-3} (9.0×10^{-4})	0.432	0.314	
	BET-TTF	1.5×10^{-2} (1.7×10^{-2})	0.326	0.246	0.021
G3	ETT-TTF	6.2×10^{-2} (3.7×10^{-2})	0.438	0.238	
	TTDM-TTF	1.5×10^{-1} (8.0×10^{-2})	0.512	0.258	0.034
	DT-TTF	2.5×10^{-1} (4.0×10^{-1})	0.574	0.238	

different tendencies of each of the TTF derivatives to form good-quality crystals and the amount of defects they contain, a notable improvement of the charge carrier mobility on going from group 1 to group 3 is observed. This trend suggests that the crystal packing of the TTF derivatives becomes more favorable from group 1 to group 3 for the preparation of OFETs. Moreover, we should especially emphasize the high mobilities found for crystals of TTDM-TTF ($\mu_{max} = 0.4 \text{ cm}^2/(\text{V}\cdot\text{s})$) and DT-TTF ($\mu_{max} = 1.4 \text{ cm}^2/(\text{V}\cdot\text{s})$), which are among the highest mobilities reported for OFETs and are the highest found for solution-processed materials.^{1,12c,29} The lower mobilities (10^{-5} – $10^{-3} \text{ cm}^2/(\text{V}\cdot\text{s})$) obtained for the TTF derivatives in group 1 are in accordance with their crystal structure since, as noted above, the formation of perpendicularly arranged dimers disrupts the intermolecular π – π interactions. These results also show that, although the crystals in group 3 are practically one-dimensional³⁰ conductors and the ones in group 2 have enhanced electronic

(27) Bürgi, L.; Richards, T. J.; Friend, R. H.; Sirringhaus, H. *J. Appl. Phys.* **2003**, *94*, 6129–6137.

(28) Mas-Torrent, M.; den Boer, D.; Durkut, M.; Hadley, P.; Schenning, A.P. *H. J. Nanotechnology* **2004**, *15*, 265–269.

(29) Katz, H. E.; Lovinger, A. J.; Johnson, J.; Kloc, C.; Siegrist, T.; Li, W.; Lin, Y.-Y.; Dodabalapur, A. *Science* **2000**, *404*, 478–481.

dimensionality and a large bandwidth,²⁴ higher hole field-effect mobilities were measured for group 3. The compounds of this group crystallize forming stacks of molecules facing one another along the device's conduction channel.

Once one has found the optimal crystal packing for OFETs based on this family of compounds, a feasible strategy to further improve this mobility might be to replace the sulfur atoms with selenium in order to promote stronger π - π interactions.

The differences in mobilities within each crystallographic group could be influenced by respective slight differences in S...S distances. However, we should note that the devices based on the molecules which present more disorder in their crystal structure due to the lower symmetry of molecules exhibit lower mobilities. Indeed, within **G3** the increase in disorder (DT-TTF < TTDM-TTF < ETT-TTF) diminishes the mobility values found. A similar tendency is observed for the molecules within groups 1 and 2. The devices based on ETT-TTF, ETTDM-TTF, BET-TTF, and ETEDT-TTF typically have high threshold voltages (i.e., the gate voltage necessary to suppress the conductivity in the crystal in the limit $V_{SD} \rightarrow 0$) and, therefore, it is not possible to turn them OFF, even when applying high positive gate voltages. This result is in agreement with the fact that the disorder induces doping in the crystal or more charge trapping at the interface between the crystal and the substrate. On the other hand, the devices based on the most symmetric molecules, DT-TTF and BEDT-TTF, show much lower threshold voltages (e.g., for DT-TTF, $0 \text{ V} < V_t < 14 \text{ V}$), with ON/OFF ratios up to 7×10^5 and 2×10^3 , respectively.

At room temperature, the charge mobility of semiconducting organic materials is often determined by a hopping transport process, which can be depicted as an electron- or hole-transfer reaction in which an electron or hole is transferred from one molecule to the neighboring one. Two major parameters determine self-exchange rates and, thus, the charge mobility:³¹ (i) the electronic coupling between adjacent molecules, which needs to be maximized, and (ii) the reorganization energy (λ_{reorg}), which needs to be small for efficient charge transport. The reorganization energy of self-exchange in a hole-hopping material is defined as the sum of the geometrical relaxation energies of one molecule upon going from the neutral-state geometry to the charged-state geometry and the neighboring molecule upon going the inverse process [$A(0) + A'(+) \rightarrow A(+) + A'(0)$]. These two portions of λ_{reorg} are typically nearly identical.³² Previous theoretical works have attempted to explain the high-mobility pentacene OFET in terms of its low λ_{reorg} .^{31b-34} We performed density functional (DF) calculations to calculate λ_{reorg} for all the studied TTF derivatives. All reported calculations were performed at the 6-31G(d,p)/B3LYP³⁵ level of theory using Gaussian 98.³⁶ In the neutral state, TTF derivatives are most energetically stable when in a distorted boat conformation but adopt planar conformation for the 1+ charged state.³⁷ First, we calculated λ_{reorg} employing the stable boat conformation for

each neutral isolated molecule and then, again, employing the closest local minimum energy structure for the neutral molecule which best approximated the conformation found in their crystal structure. For group 2 and group 3 crystal structures, the constituent TTF derivatives are found to be almost perfectly planar. Thus, in our calculations, to represent this packing-induced planarity, isolated neutral molecules were optimized to local energetic minimum planar conformations. For the group 1 crystal packing, the TTF derivatives are not planar but adopt boatlike conformations. For BEDT-TTF we employed the lowest energy boat conformation, and, in the case of ETEDT-TTF, a minimum energy structure very close to the lowest energy boat conformation was found to be the best isolated molecular representation. For each calculation, the lowest energy planar 1+ molecular conformation was used. These results are summarized in Table 1. Comparing the resulting λ_{reorg} values of all these molecules, we find that λ_{reorg} values calculated while always employing the lowest energy neutral molecule boat conformations do not follow any obvious pattern relating to the corresponding crystal structure. However, when the calculations are done employing the isolated neutral conformations, approximating the crystal packing-constrained molecular geometries, a trend of λ_{reorg} values emerges in line with that of the experimentally measured mobilities; i.e., molecules with better mobilities tend to have lower λ_{reorg} values. The main reason for the difference in these two sets of calculations comes from the use of planar neutral molecules to represent the respective planar TTF derivatives in the crystals of groups 2 and 3, which results in a notable drop of λ_{reorg} . This decrease in the λ_{reorg} values can be simply explained by the fact that the geometries of the neutral and charged planar molecules become closer, which is not the case for molecules of group 1. The calculated differences in isolated molecular λ_{reorg} values, however, do not appear to fully explain the relatively large measured differences found in the mobilities, suggesting that intermolecular interactions should also be taken into account.

As mentioned above, the other parameter that determines mobilities, in addition to the reorganization energy, is the intermolecular electronic coupling, often estimated via the calculation of transfer integrals.³⁸ In Table 1, we thus further report transfer integrals for the TTF derivative crystals displaying the highest mobility (and highest symmetry) in each crystal structure group. The single value, t_{max} , quoted for each group is the maximum transfer integral for that crystal, based on a systematic search of all nearest-neighbor dimeric possibilities for the strongest electronic coupling. Remarkably, the transfer integral values also follow the trend found for the experimentally measured mobilities; i.e., the crystals with higher mobilities also have higher maximum transfer integrals. For DT-TTF, t_{max} is

(30) Rovira, M. C. Ph.D. Thesis, University of Barcelona, Barcelona, Spain, 1995.

(31) (a) Marcus, R. A. *Rev. Mod. Phys.* **1993**, *65*, 599. (b) Gruhn, N.; E.; da Silva Filho, D. A.; Bill, T. G.; Malagoli, M.; Coropceanu, V.; Kahn, A.; Brédas, J.-L. *J. Am. Chem. Soc.* **2002**, *124*, 7918–7919.

(32) Malagoli, M.; Brédas, J. L. *Chem. Phys. Lett.* **2000**, *327*, 13–17.

(33) Cornil, J.; Calbert, J. Ph.; Brédas, J. L. *J. Am. Chem. Soc.* **2001**, *123*, 1250–1251.

(34) Meng, H. M.; Bendikov, M.; Mitchell, G.; Helgeson, R.; Wudl, F.; Bao, Z.; Siegrist, T.; Kloc, C.; Chen, C.-H. *Adv. Mater.* **2003**, *15*, 1090–1093.

(35) Becke, A. D. *J. Phys. Chem.* **1993**, *98*, 5648.

(36) Frisch, M. J.; Trucks, G. W.; Schlegel, H. B.; Scuseria, G. E.; Robb, M. A.; Cheeseman, J. R.; Zakrzewski, V. G.; Montgomery, J. A., Jr.; Stratmann, R. E.; Burant, J. C.; Dapprich, S.; Millam, J. M.; Daniels, A. D.; Kudin, K. N.; Strain, M. C.; Farkas, O.; Tomasi, J.; Barone, V.; Cossi, M.; Cammi, R.; Mennucci, B.; Pomelli, C.; Adamo, C.; Clifford, S.; Ochterski, J.; Petersson, G. A.; Ayala, P. Y.; Cui, Q.; Morokuma, K.; Malick, D. K.; Rabuck, A. D.; Raghavachari, K.; Foresman, J. B.; Cioslowski, J.; Ortiz, J. V.; Stefanov, B. B.; Liu, G.; Liashenko, A.; Piskorz, P.; Komaromi, I.; Gomperts, R.; Martin, R. L.; Fox, D. J.; Keith, T.; Al-Laham, M. A.; Peng, C. Y.; Nanayakkara, A.; Gonzalez, C.; Challacombe, M.; Gill, P. M. W.; Johnson, B. G.; Chen, W.; Wong, M. W.; Andres, J. L.; Head-Gordon, M.; Pople, J. A. *Gaussian 98*, revision A.9; Gaussian, Inc.: Pittsburgh, PA, 1998.

(37) Demiralp, E.; Goddard, W. A., III. *J. Phys. Chem. A* **1997**, *101*, 8128–8131.

(38) Brédas, J. L.; Calbert, J. P.; da Silva Filho, D. A.; Cornil, J. *Proc. Natl. Acad. Sci. U.S.A.* **2002**, *99*, 5804–5809.

found along the packing crystal axis *b*, which also corresponds to the long crystal direction and, thus, the device channel direction. However, for BET-TTF, whereas the long crystal axis is known to correspond to the crystallographic *b* + *c* direction, t_{\max} is found between the lateral S \cdots S contacts present in the *ab* plane. Finally, for BEDT-TTF, the interdimer t_{\max} is also found to be between the lateral S \cdots S along the *a* axis.

The extremely encouraging trends in both λ_{reorg} and t_{\max} values are thus far based on calculations made employing isolated molecules/dimers. Such studies can further benefit by taking into account a fuller representation of the true crystal environment; e.g., the boat conformations in the crystals of group 1 are stabilized by intermolecular hydrogen bonding. Previously, we demonstrated that an additional drop in the λ_{reorg} value of DT-TTF is observed if one considers crystal-embedded molecules rather than using solely their isolated planar molecular representations.³⁹ In this way, we hope in the future to further investigate the role of intermolecular interactions on TTF derivative crystal transport properties.

Conclusions

In conclusion, the facile processing and easy chemical modification of TTF derivatives has permitted us to systematically investigate the influence of the crystal structure on the performance of single-crystal OFETs. A trend in mobilities through the different crystal structures is observed which is further strongly corroborated by calculations of both the molecular reorganization energies and the maximum intermolecular transfer integrals. Among the structures studied here, the herringbone crystal structure of materials in group 3 showed the best performance for OFETs. The devices of this group exhibit the highest mobilities found for solution-processed materials and are also among the highest reported for OFETs. These mobility values are of the order of that of amorphous silicon, which is widely used in solar cells and flat-screen displays. This result responds to the current need to find materials which show high mobilities and are solution-processed and, therefore, are particularly suitable for low-cost electronics. Future work will be directed to further study this family of compounds and try to improve the mobilities either by improving the devices or by searching for new derivatives.

Experimental Section

BEDT-TTF was purchased from Aldrich, and ETEDT-TTF,²¹ BET-TTF,²² DT-TTF,²² and ETT-TTF²⁶ were synthesized as previously described. ETTDM-TTF and TTDM-TTF were synthesized as follows.

ETTDM-TTF. To a 10 mL flask were added 0.11 g (0.62 mmol) of 5,6-dihydrothieno[2,3-*d*]-1,3-dithiol-2-ketone⁴⁰ and 0.12 g (0.62 mmol) of 4,6-dihydrothieno[3,4-*d*]-1,3-dithiol-2-thione.²² After the addition of 3 mL of dry P(OMe)₃ (freshly distilled), the mixture was refluxed under argon for 4 h. After the mixture cooled to room temperature, the red crystals that formed were filtered, washed with diethyl ether, and dried under a vacuum. The desired compound was obtained without contamination of the respective symmetric compounds in a 47% yield (94 mg). UV/vis (CHCl₃): $\lambda_{\text{max}}/\text{nm}$ ($\epsilon/\text{cm}^{-1} \text{ M}^{-1}$) = 311 (14 000), 338 (sh, 10 700), 467 (340). IR (KBr pellet): ν/cm^{-1} = 2938, 2903, 2833, 1432, 1298, 1258, 1235, 1150, 1136, 1114, 1098, 1075, 1014, 999, 882, 765, 715, 454. FAB-MS: m/e = 320 (C₁₀H₈S₆,

M⁺, 100%). ¹H NMR (CDCl₃, referenced to TMS): δ/ppm = 2.86 (t, 2H, CH₂-S), 3.75 (t, 2H, CH₂-C), 3.76 (s, 4H, CH₂-S-CH₂). ¹³C NMR (CDCl₃, referenced to TMS): δ/ppm = 32.9 (C-CH₂-CH₂), 34.2 (C-CH₂-S), 38.4 (S-CH₂-CH₂), 122.6 (S-C-CH₂-CH₂), 125.8 (S-C-S), 130.4 (S-C-CH₂-S). Cyclic voltammetry (DMF, 298 K, vs Ag/AgCl): $E_{1/2}^1$ = 0.49 V, $E_{1/2}^2$ = 0.68 V.

TTDM-TTF. A mixture of 0.10 g (0.5 mmol) of 4,6-dihydrothieno[3,4-*d*]-1,3-dithiol-2-thione,²² 0.1 g (0.5 mmol) of [3,4-*d*]-1,3-dithiol-2-thione,⁴¹ and 3 mL of dry P(OMe)₃ (freshly distilled) was refluxed in a 10 mL flask under argon for 3.5 h. The mixture was allowed to cool to room temperature and then was filtered; the yellowish solid was washed with diethyl ether and dried under a vacuum. The mixture, containing the disymmetric desired compound and the symmetric DT-TTF, was chromatographed with silica using CS₂ as solvent, finally obtaining 8 mg of pure TTDM-TTF in a 5% yield. UV/vis (CHCl₃): $\lambda_{\text{max}}/\text{nm}$ ($\epsilon/\text{cm}^{-1} \text{ M}^{-1}$) = 288 (sh, 2500), 316 (3200), 436 (315). IR (KBr pellet): ν/cm^{-1} = 3099, 2913, 2841, 1499, 1434, 1321, 1232, 1153, 1136, 1109, 1023, 874, 831, 766, 749, 714, 700, 669, 507, 467, 455, 441. FAB-MS: m/e = 318 (C₁₀H₆S₆, M⁺, 100%). ¹H NMR (CDCl₃, referenced to TMS): δ/ppm = 3.77 (s, 4H, -CH₂-S-CH₂), 6.88 (s, 2H, -CH-S-CH₂). ¹³C NMR (CDCl₃, referenced to TMS): δ/ppm = 34.2 (C-CH₂-S), 112.1 (S-CH-C), 130.0 (S-C-CH₂), 136.0 (CH-C-S). Cyclic voltammetry (DMF, 298 K, vs Ag/AgCl): $E_{1/2}^1$ = 0.62 V, $E_{1/2}^2$ = 0.82 V.

Crystallographic Data. X-ray-quality dark-red thin platelike crystals of ETTDM-TTF and yellow thin platelike crystals of TTDM-TTF were obtained by slow diffusion of pentane in a CS₂ solution and by slow evaporation of a CH₂Cl₂ solution, respectively.

Crystal data for ETTDM-TTF: C₁₀H₈S₆, M = 320.53, triclinic $P\bar{1}$, a = 6.379(3) Å, b = 7.835(9) Å, c = 12.300(10) Å, α = 102.53(6)°, β = 93.15(6)°, γ = 92.89(6)°, V = 598.0(9) Å³, Z = 2, ρ_{calcd} = 1.780 mg m⁻³, T = 293(2) K, R = 0.0522, $wR2$ = 0.1583, GOF = 1.055 ($I > 2.0\sigma(I)$).

Crystal data for TTDM-TTF: C₁₀H₆S₆, M = 318.52, monoclinic $P2_1/c$, a = 13.9760(10) Å, b = 4.10900(10) Å, c = 10.9270(10) Å, β = 110.118(7)°, V = 589.22(7) Å³, Z = 4, ρ_{calcd} = 1.795 mg m⁻³, T = 293(2) K, R = 0.0342, $wR2$ = 0.0852, GOF = 1.052 ($I > 2.0\sigma(I)$).

Data Collection. Crystals were mounted in an Enraf-Nonius CAD4 diffractometer with a graphite monochromator and Mo K α radiation at 293(2) K. Unit cell parameters were determined from a least-squares analysis of 25 reflections. In both cases, intensity data were collected by the zigzag ρ - 2θ scan technique with no fluctuations in standard reflections. The index ranges were $0 \leq h \leq 9$, $-11 \leq k \leq 11$, $-17 \leq l \leq 17$ for ETTDM-TTF and $0 \leq h \leq 19$, $0 \leq k \leq 5$, $-15 \leq l \leq 14$ for TTDM-TTF. For ETTDM, 3603 reflections were collected, of which and 2676 were unique. For TTDM-TTF, 1786 reflections were collected, of which 1179 were unique. In both cases, L_p correction was applied, but no corrections for absorption were done. The structures were solved by direct methods (SHELXS86) and refined against F^2 (SHELX97),⁴² using anisotropic thermal parameters for the non-H-atoms and one global isotropic temperature factor for the H-atoms. Scattering factors were taken from the *International Tables for X-ray Crystallography*,⁴³ except for those of the H-atoms.⁴⁴

Device Preparation. Silicon substrates with a 200 nm thermally grown oxide layer were purchased from Wacker Siltronic AG. Electrode fabrication was carried out in an electron beam pattern generator (EBPG5 HR 100 kV FEG) using a double poly(methyl methacrylate) (PMMA) resist. Four nanometers of Ti and 20 nm of Au were evaporated at liquid nitrogen temperature to ensure a smooth surface, and lift-off was done in acetone.

(39) Bromley, S. T.; Mas-Torrent, M.; Hadley, P.; Rovira, C. *J. Am. Chem. Soc.* **2004**, *126*, 6544–6545.

(40) Pérez-Benítez, A.; Tarrés, J.; Ribera, E.; Veciana, J.; Rovira, C. *Synthesis* **1999**, *4*, 577–579.

(41) Chiang, L.-Y.; Shu, P.; Holt, D.; Cowan, D. *J. Org. Chem.* **1983**, *48*, 4713–4717.

(42) Sheldrick, G. M., *SHELXL97: Program for the refinement of crystal structures*; University of Göttingen: Göttingen, Germany, 1997.

(43) *International Tables for X-ray Crystallography*; Kynoch Press: Birmingham (present distributor D. Reidel, Dordrecht), 1984; Vol. IV, pp 99–149.

(44) Stewart, R. F.; Davidson, E. R.; Simpson, W. T. *J. Chem. Phys.* **1965**, *42*, 3175.

The single-crystal transistors were prepared by heating a saturated solution of the corresponding TTF derivative in chlorobenzene at about 60 °C and pouring it over the substrates containing the microfabricated electrodes at room temperature. The solvent was allowed to evaporate very slowly for about 2 h in a sealed container, giving rise to good-quality long plate crystals, some of which bridged the electrodes.

Transport Measurements. The transport measurements were carried out in a Probe Station Microscope coupled to an ADwin Gold external data acquisition system in darkness. An optical microscope, Olympus DP10, was also used to inspect the samples.

Density Functional Calculations. All DFT calculations were performed using the Gaussian 98 code.³⁶ The electronic coupling between adjacent TTF molecules in the crystal was estimated by the method described in ref 38. Two DFT-optimized TTF molecules (in the approximated crystal structure conformation) were placed at the

respective neighboring crystal positions. The splittings of the HOMO levels due to this configuration were then calculated using the INDO/S Hamiltonian. Half of the calculated splitting gives an estimate of the transfer integral.

Acknowledgment. This work was supported by DGI, Ministerio de Ciencia y Tecnología, Spain (Project BQU2003-00760), and DGR, Generalitat de Catalunya (Centre de Referencia CeRMAE and Project 2001SG00362). M.M.-T. also thanks DGR for a nanotechnology fellowship.

Supporting Information Available: X-ray crystallographic files for ETTDM-TTF and TTDM-TTF (CIF). This material is available free of charge via the Internet at <http://pubs.acs.org>. JA048342I